Biomed Microdevices (2008) 10:653–660
DOI 10.1007/s10544-008-9176-5

Handheld subcellular-resolution single-fiber confocal microscope using high-reflectivity two-axis vertical combdrive silicon microscanner

Karthik Kumar · Kazunori Hoshino · Xiaojing Zhang

Published online: 1 May 2008

Abstract We introduce a handheld single-fiber laser-scanning confocal microscope, incorporating a high-reflectivity two-axis silicon vertical combdrive microscanner, aimed at *in vivo* early detection of epithelial precancers. The approach adopted is motivated by need for a portable, economical, biopsy-free, early precancer screening technology in low-infrastructure environments. Our microelectromechanical system (MEMS) based handheld probe integrates the microscanners with miniature objective lens system and flexible electrical routing in a forward-imaging configuration, with 4.8 mm distal probe tip outer diameter for unrestricted imaging access in biological sites such as the oral cavity and cervix. Reflectance confocal videos of a USAF 1951 resolution target and biological samples were obtained over 200 μm×110 μm field of view, with 0.80 and 9.55 μm lateral and axial resolution, at 3.5–5.0 frames per second. With improvements to objective numerical aperture, our probe can enable precise evaluation of nuclear size, density, nucleus-to-cytoplasm ratio and cell density, which are important visual identifiers of epithelial precancers.

K. Kumar (✉)
Department of Electrical and Computer Engineering,
University of Texas at Austin,
Austin, TX 78712, USA
e-mail: kkumar@mail.utexas.edu

K. Hoshino · X. Zhang
Department of Biomedical Engineering,
University of Texas at Austin,
Austin, TX 78712, USA

X. Zhang
e-mail: John.Zhang@engr.utexas.edu

Keywords Microelectromechanical systems · Two-axis microscanner · Confocal microscopy · Handheld probe · Biomedical diagnostics · Subcellular imaging

1 Introduction

Demographic data indicates that 60% of the 6.7 million annual global cancer mortalities, and 54% of 10.8 million new patients are in developing nations (Cancer Research UK 2005), unable or unwilling to avail of invasive histopathologic screening. However, histopathologic examination by reflectance confocal microscopy has shown subcellular morphological changes (nuclear size, density, nuclear-cytoplasmic ratio) to be unambiguous identifiers of epithelial precancers (Carlson 2006; Collier et al. 2000; McKinnell et al. 2006), from which 85% of cancers originate. Also, local early detection and treatment dramatically improves patient survival chances (American Cancer Society 2007). These factors dictate the development of a portable, low-power, point-of-care *in vivo* reflectance confocal microscope capable of subcellular resolution required to visualize morphological changes associated with epithelial precancers without biopsy in underdeveloped infrastructure environments.

Miniaturization of optical diagnostic equipment is critical for translation of *in vitro* histopathologic examination to *in vivo* diagnostics in clinical medicine. Several approaches have been adopted to perform confocal microscopy in compact form factor. A fiber-optic bundle comprising thousands of closely-spaced single-mode fibers packaged with an objective lens has been used for *in vivo* confocal imaging by selecting, at the proximal end, the fiber through which illumination is directed, and scanning

through all the fibers sequentially (Carlson et al. 2005; Gmitro and Aziz 1993; Rouse et al. 2004). Though significant miniaturization is achieved, the method suffers from pixilation imaging artifact and lowered spatial resolution due to finite spacing between adjacent fiber cores. Microelectromechanical system (MEMS) technologies offer the unique capability to package micro-optical elements with actuators to perform beam-scanning at the distal end for imaging within *in vivo* environments. Distal-end scanning can be performed by fiber/objective translation, or by micromirror-based angular beam deflection. Piezoelectric actuators (Dabbs and Glass 1992; Flusberg et al. 2005) and tuning forks (Polglase et al. 2005) have been used to translate the fiber relative to a stationary objective lens to scan the illumination across the sample. The drawback of these techniques is that the fiber end must be scanned a distance proportionately greater than the field-of-view, or FOV (given by the demagnification ratio of the objective lens). Scanning the objective relative to the stationary fiber (Dickensheets and Kino 1996; Giniunas et al. 1991) eliminates this problem; however, scanning the relatively bulky lens is slow and energy-inefficient. Silicon micromachined torsional scanning mirrors providing angular beam deflection using parallel plate actuation have been used in microfabricated laser-scanning confocal microscopes (Dickensheets and Kino 1998). Recently developed lateral (Zhou et al. 2006), angular (Hah et al. 2004), and vertical (Krishnamoorthy et al. 2003; Kumar et al. 2006; Kwon et al. 2004) electrostatic comb-driven scanning micromirrors provide larger actuation torque, deflection angles, and better voltage pull-in characteristics compared with parallel plate actuation schemes. Such scanning micromirrors have previously been employed in optical coherence tomography (Pan et al. 2001; Xie et al. 2003), two-photon microscopy (Piyawattanametha et al. 2006), dual-axes confocal microscopy (Liu et al. 2007; Ra et al. 2007), and bench-top single-fiber laser-scanned confocal microscopy (Maitland et al. 2006). Here we introduce a portable, handheld, single-fiber reflectance confocal microscope employing a two-axis vertical combdrive scanning micromirror with significantly enhanced reflectivity, demonstrating subcellular resolution imaging aimed at *in vivo* early detection of epithelial precancers. Comparing to recent work on bench-top single-fiber confocal microscopy using a two-axis MEMS scanner (Shin et al. 2007), our handheld probe visualizes larger field of view (200 μm × 110 μm) with comparable lateral and axial resolution (0.80 and 9.55 μm respectively) at 3.5–5.0 frames per second, all within a 15 mm^3 package. Videos of resolution target, *in vitro* porcine oral tissue, and *in vivo* human fingernail demonstrate its promise towards endoscopic oral and cervical precancer detection.

2 Design and fabrication of probe subsystems

2.1 Scanning micromirror

The micromirror that raster scans the incident illumination across the objective lens system plays a critical role in miniaturizing the probe. We employed an electrostatic staggered vertical comb drive design that provides high actuation torque, large deflection angles, low dynamic mirror deformation and favorable voltage pull-in characteristics. Our mirrors have dimensions of 500 μm × 700 μm for illumination at 45° incidence by a 500 μm diameter laser beam, and are coated with 125 nm of silver to improve reflectivity at 635 nm wavelength from 29% (for bare silicon) to over 90%.

Figure 1(a) outlines the silicon micromachining process used to fabricate the scanning mirrors. Coarse features of stationary electrostatic actuating comb drives are etched by Deep Reactive Ion Etching (DRIE) into the 30 μm conductive device layer of a Silicon-On-Insulator (SOI) wafer. A separate silicon wafer is oxidized to form an electrical isolation layer, fusion-bonded on top of the SOI wafer, ground down to 20 μm thickness, and polished to give a smooth (less than 50 nm RMS surface roughness) optical surface. The mirror and rotor combs are fabricated in this layer. A layer of silicon dioxide 1.5 μm thick serving as silicon etch hard mask is deposited by Low Pressure Chemical Vapor Deposition (LPCVD). After dry etching through the top device layer to expose alignment marks in the lower silicon layer, electrical bond pad features are etched partially (1.2 μm) and the exact features of the microscanners are etched through the oxide layer by Reactive Ion Etching (RIE). The oxide layer is used as an etch mask then to perform a DRIE–Oxide RIE–DRIE etch sequence to create the rotor comb features, bond pad vias to the lower silicon layer, and trim the underlying stator combs to match the lateral position of the stator comb features. This self-aligning technique (Krishnamoorthy et al. 2003; Kumar et al. 2006) affords a critical mask misalignment tolerance of half the comb width (3.0 or 3.5 μm in our case) and ensures stable and reliable scanner operation with minimal stiction. DRIE is used to create a backside window underneath the device to release the micromirror using the buried oxide layer of the SOI wafer as an etch stop, while simultaneously dicing the wafer into device chips. Remaining exposed oxide is removed from the front and backside by RIE. A <100> silicon wafer is anisotropically wet etched in potassium hydroxide using a silicon nitride masking layer at 70°C to create a sputter hard mask. Using this hard mask, the micromirrors are selectively coated with 125 nm of silver by electron beam evaporation to improve mirror reflectivity. Scanning electron micrographs of the fabricated microscanners, vertical

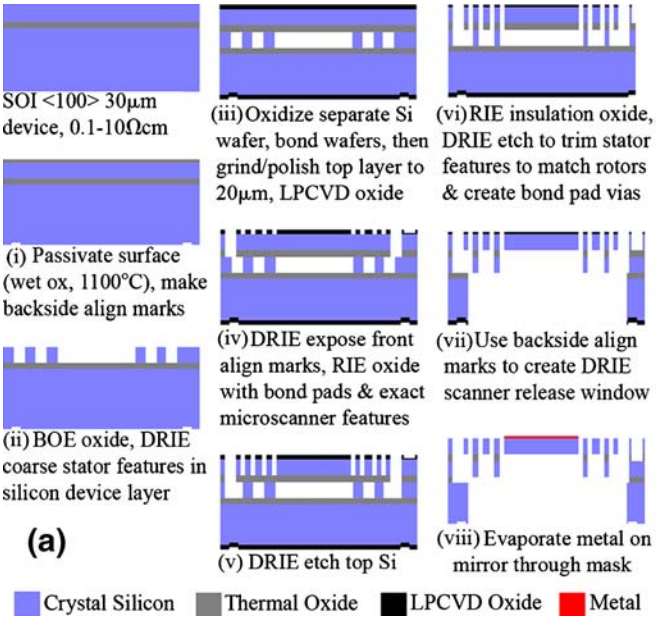

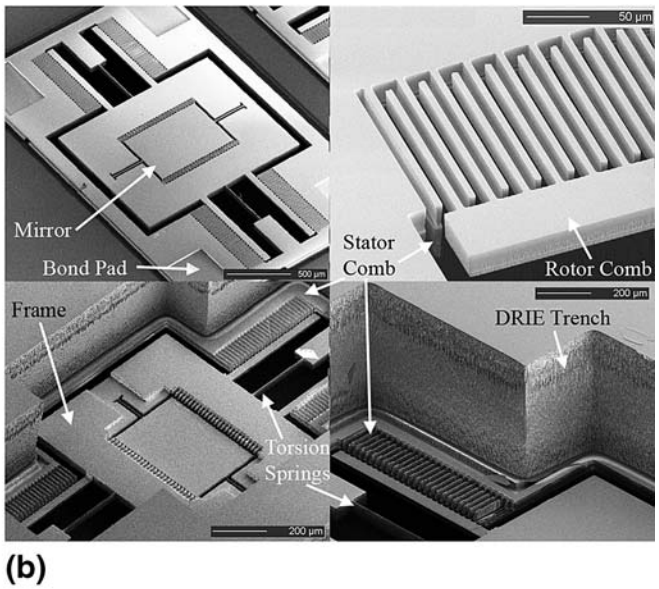

Fig. 1 High-reflectivity two-axis vertical combdrive microscanners. (**a**) Process flow for device fabrication, (**b**) Scanning electron micrographs (SEM) of fabricated microscanners depicting mirror and frame design, torsion springs, stator and rotor combs, bond pads, and backside DRIE released window

comb drives, and backside DRIE trench are shown in Fig. 1(b).

The measured micromirror static-voltage and frequency-dependent deflection characteristics are depicted in Fig. 2. The maximum angular deflection obtained in static-voltage mode is limited to ~9° (for single-sided actuation) by the voltage pull-in characteristics of the microscanner, and is lower than those achieved in resonant scanning mode. We attribute this to reduced lateral stiffness of the springs due to over-etching.

The resonant frequencies, 2.28 kHz for inner axis and 383 Hz for outer axis, are in good agreement with values calculated by Finite Element Modeling simulations using CoventorWare™. The measured frequency response curve of inner and outer axis shows three peaks for each rotation axis at $\omega_0/2$, ω_0, and $2\omega_0$ (ω_0 is the fundamental resonant frequency of the vibration modeshape) as expected (Lee 2007).

2.2 Miniature objective

The miniature objective lens system used was previously reported in (Shin et al. 2007). It is designed in Keplerian telescope configuration with 3 mm diameter lenses mounted in a three-piece metal housing of 36.05 mm length and 4.77 mm outer diameter. The first two lenses (achromatic, f=4.5 mm/12.0 mm, Edmund Optics) create 2.67X beam expansion, providing 0.33 effective NA (for 500 μm input beam diameter) propagating into the third lens of the objective system (aspheric, f=2.0 mm, Thorlabs, Inc.). The lens-micromirror system provides 0.80 μm lateral and 9.55 μm axial resolution.

2.3 Forward-imaging MEMS handheld probe prototype

A forward-imaging probe is expected to be better suited for handheld confocal microscopy of epithelial tissue in the oral cavity and cervix as compared to a sideways-imaging probe. Accordingly, we have designed and constructed a 15 mm^3 aluminum-milled MEMS packaging cube with built-in stationary mirror, microscanner chip mount, optics ports for input pigtailed collimator, miniature Keplerian telescope objective system, and an electrical routing port to the microscanner. Schematics and photographs of the package we developed are shown in Fig. 3. The positions of the centers of the optics ports, the 45° angled stationary mirror and the center of one of the four micromirrors on the microscanner chip are aligned precisely for easy assembly. The stationary mirror reflectivity, hence the imaging resolution, can be improved by coating a layer of silver of thickness 125 nm on top of the aluminum. Polycarbonate rings with screws are attached on to each optic port on the inside of the package to fasten the miniature optics inserted into the system. Future embodiments of the instrument will incorporate micro-optical phase control elements, such as the quarter-wave plate (QWP), to further minimize the impact of spurious reflections in the optical system.

2.4 Flexible electrical routing

To ensure complete maneuverability of the device during operation, we developed electrical traces on flexible Kapton substrate to deliver power to the microscanner within the MEMS package. Kapton is a tough material, resistant to

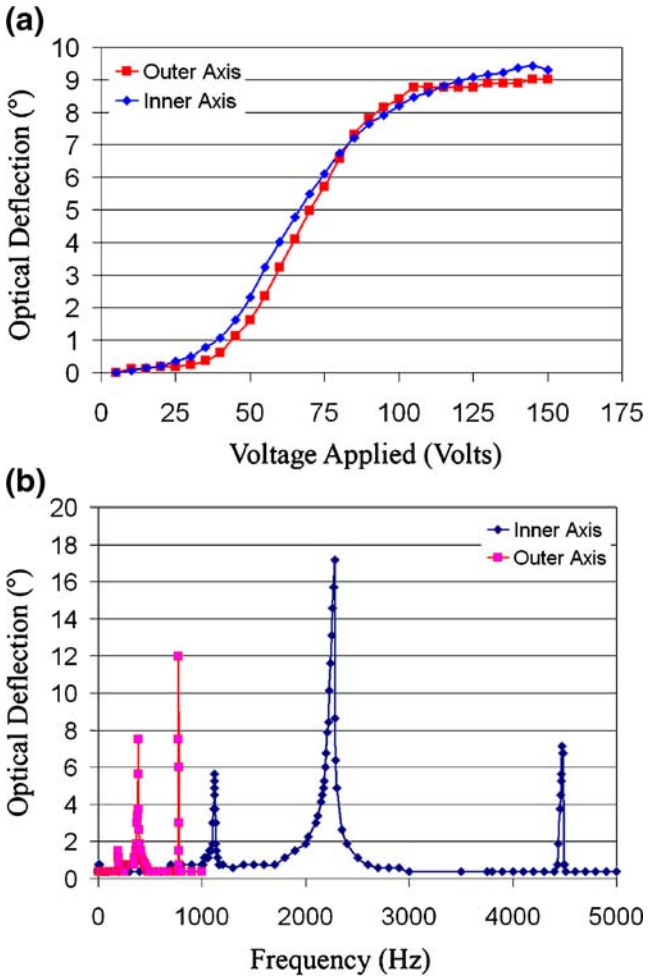

Fig. 2 Microscanner operating characteristics. (**a**) Single-sided static voltage deflection characteristics, (**b**) Frequency-dependent optical deflection. Applied voltage, $V = 18.0 + 9.0\sin(2\pi ft)$ volts

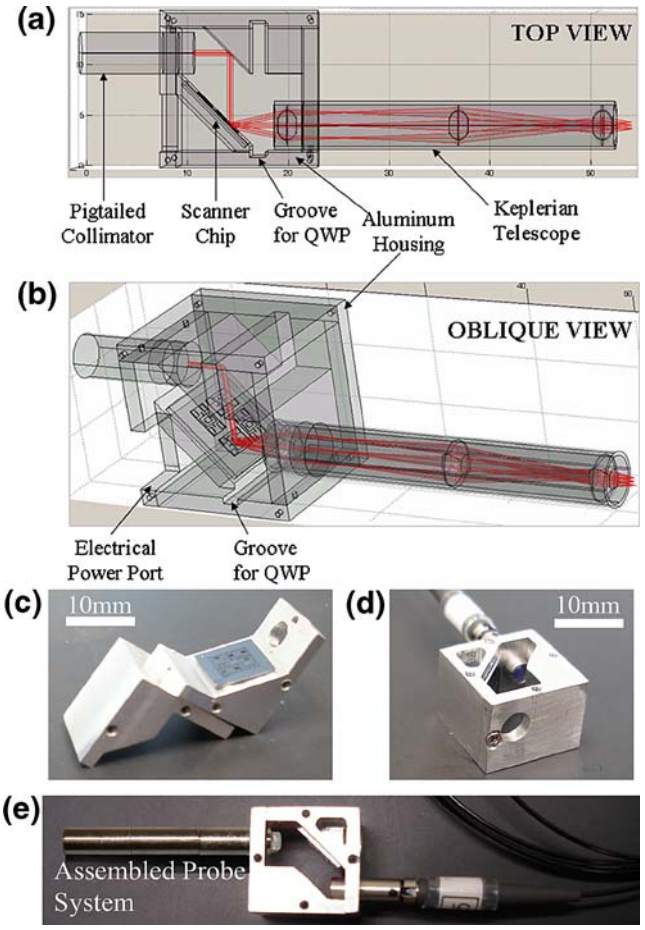

Fig. 3 The handheld MEMS probe package. (**a**) *Schematic top view* of layout, depicting optical components and light path, (**b**) *Oblique view* of the MEMS packaging scheme, (**c**) Photograph of the two blocks forming part of the package, with microscanner chip mounted, (**d**) Assembled package with pigtailed collimator inserted into the input optical port, (**e**) Full mechanical probe assembly (*top and bottom* cover plates of the package not shown in images)

shear stress, and can withstand the high temperatures required in semiconductor processing. The fabrication process begins with pre-coating 30 μm thick copper layer on 125 μm thickness Kapton substrate, which is subsequently patterned using photolithography and wet etched using Ferric Chloride solution. After trimming the substrate, the cable is inserted through the electrical port in the package and adhered using epoxy to the microscanner chip. Gold wires of 25 μm diameter are wire-bonded between the copper traces and the exposed stator layer of silicon in the microscanner bond pad vias (Fig. 4). Stranded wires soldered to the proximal end of the flexible routing complete circuitry.

3 Instrument operation and characterization

The MEMS confocal probe is integrated into a reflectance confocal microscopy experiment as depicted in Fig. 5. A solid state semiconductor laser provides linearly-polarized 635 nm wavelength illumination guided to the probe using polarization-maintaining fiber. The QWP, with optic axis aligned at 45° angle to the incident polarization, and the polarizing beamsplitters, ensure that any reflection in the system occurring before propagation though the QWP does not reach the avalanche photodiode receiver. The microscanner deflects the beam across the sample in raster fashion. The inner axis of the scanner is operated at resonance to perform fast line scans, while the outer axis is operated at low frequency for the frame scan. Table 1 lists the operating parameters of the microscanner. The extremely low current values required for operation on both axes indicate that the system can be battery-powered (with appropriate voltage transformation circuitry) for operation in low-infrastructure environments.

In acquiring reflectance confocal video of a positive USAF 1951 resolution target, we observed a field-of-view

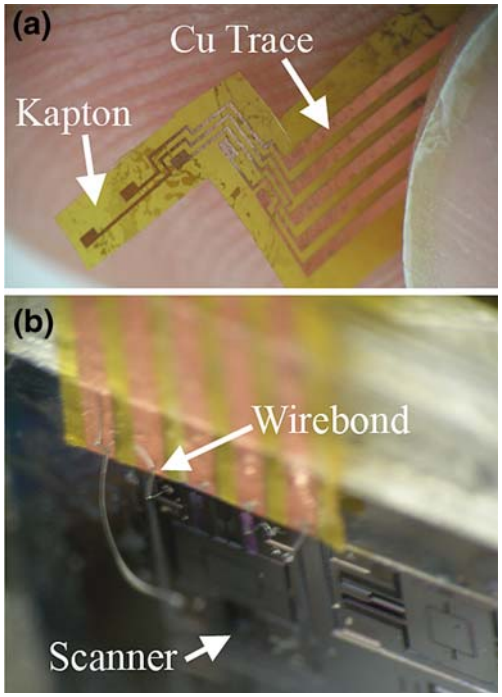

Fig. 4 Flexible electrical routing circuit. (**a**) Photograph of copper electrical traces fabricated on flexible Kapton substrate, (**b**) Photograph of wire-bonding connections made between the flexible routing traces and the silicon stator layer on microscanner chip

of 200 μm×110 μm at 3.5–5.0 frames per second. The field of view was achieved by actuating the slow axis with both sets of vertical comb drive actuators. Instability in the slow scan was observed when each comb was actuated downwards to one side, while the retrace to equilibrium position was extremely stable. Therefore, for a full period of the double-sided scan, the first and third quarters of the scan were combined (after laterally inverting the lines obtained during the third quarter), while the second and fourth quarters of the scan were rejected. Figure 6(a) shows one a frame from a video acquired in this manner, in which all the elements of group 7 and some elements of group 6 are visible. The smallest bars among the group 7 elements of 2.2 μm width are clearly resolved, demonstrating that the system is capable of the sub-cellular resolution required for imaging of nuclei of 10–20 μm diameter epithelial cells. We also acquired videos of *in vitro* oral porcine tissue treated with acetic acid for improved contrast (Drezek et al. 2000), and *in vivo* human fingernail (Fig. 7).

4 Discussion and performance analysis

Our experiments with a handheld MEMS-based single-fiber reflectance confocal microscope probe demonstrate that scanning micromirrors integrated with single-mode fiber optics and miniature optical elements can provide sub-cellular imaging resolution in a compact form factor. Further miniaturization can be achieved without sacrificing imaging performance by building one microscanner device to a chip (4× reduction in space), and using a fiber-fused, graded index (GRIN) lens collimator with smaller diameter and micro-prism stationary reflector in place of the pigtailed collimator and aluminum-machined stationary mirror used in the current prototype. Fabrication tolerances allowed in machining this first-generation MEMS package prototype can also be reduced to achieve modest improvements in form factor. Rapid prototyping alternatives to aluminum machining such as laser stereolithography (Cooke et al. 2002; Scarparo et al. 1996) can be employed for batch-fabrication with improved turnaround time. Mechanisms to reduce motion blur experienced while imaging live subjects *in vivo* can also be included. Hydraulic suction systems have been previously demonstrated to hold the sample against the objective, and

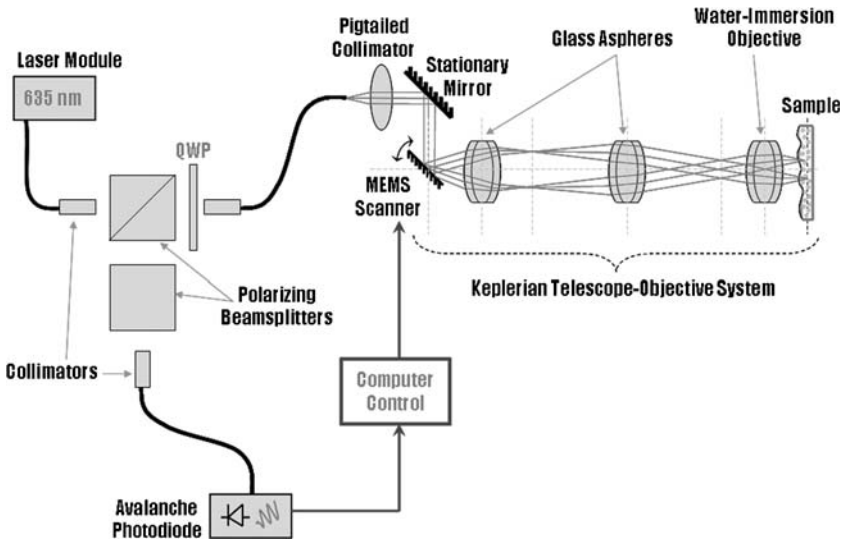

Fig. 5 Schematic of single-fiber laser-scanning reflectance confocal microscopy experiment incorporating the handheld MEMS probe

Table 1 Microscanner operating parameters and characteristics

Axis	Scan mode	Driving freq. (Hz)	Applied voltage, $V=V_{DC}+V_{PP}\sin(\omega t)$		I_{RMS} (μA)	Opt. angle (°)
			V_{DC} (V)	V_{PP} (V)		
Inner	Resonant	2,755.0	20.0	10.0	2.4	18.0
Outer	Nonresonant	3.5–5.0	82.5	47.5	0.05	9.5

perform axial scanning. Such systems may increase the outer diameter of the distal tip, but will provide important functionality in clinical usage.

The MEMS microscanner plays a critical role in determining the resolution and contrast of the reflectance confocal microscope. Higher values of numerical aperture (NA) of the objective system are required to obtain better optical sectioning in highly scattering tissue samples. The relatively low NA of our system [0.33, as compared to a prescribed value of 0.7–1.2 for optimal optical sectioning (Rajadhyaksha et al. 1999)] accounts for the reduced contrast in the biological imaging. The product of the micromirror size and its optical deflection angle determines the number of resolvable points in the image (Webb 1984), which translates into a given field-of-view and resolution according to the numerical aperture selected for the objective system. Therefore, using a higher NA objective without modifying the scanner deflection angles will improve lateral (and axial) resolution but reduce the field-of-view proportionately. Micromirrors with larger dimensions providing the same deflection angles can be designed with marginal increase in energy consumption (to actuate the larger mirror). Based on our measurements of the current drawn by the scanner (Table 1), this is a favorable trade-off that we can afford in the system design.

We have developed our handheld probe for single-fiber laser-scanning subcellular-resolution reflectance confocal microscopy, with a view to detecting precancer *in vivo* based on direct visualization of morphological changes in diseased tissue. Several previous studies have focused on developing fluorescent molecular beacons conjugated to

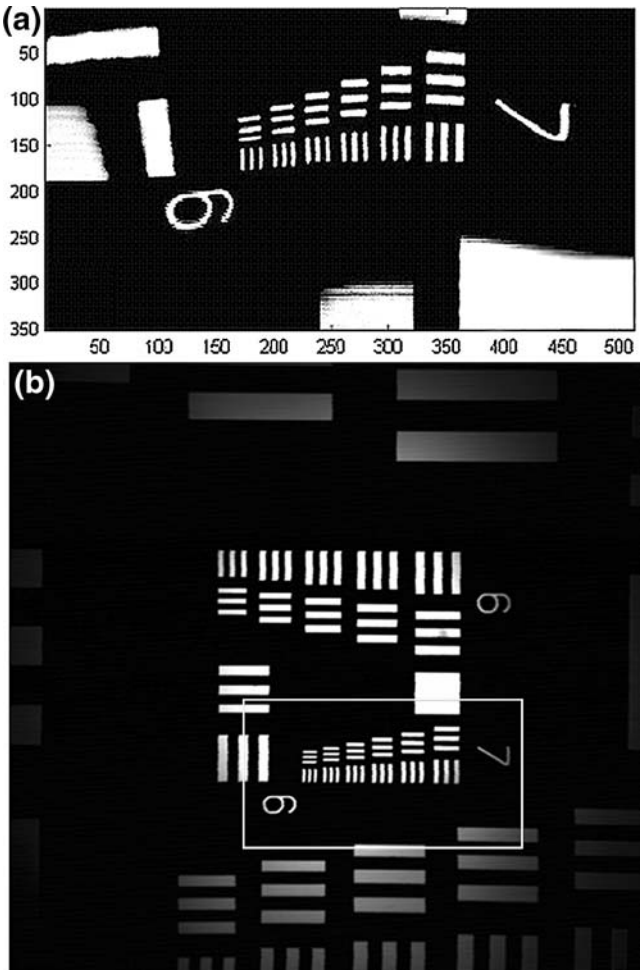

Fig. 6 MEMS Confocal images of a USAF 1951 resolution target. (**a**) Image of group 7 elements, and some elements of group 6. Field of view is 200 μm×110 μm. The *smallest bars* of group 7 are of width 2.2 μm, (**b**) Image of the resolution target obtained using a commercial confocal microscope (Lucid VivaScope 2500) with field of view 500 μm×500 μm. The region in (**b**) enclosed in the *white rectangle* represents the area imaged using our handheld reflectance confocal microscope

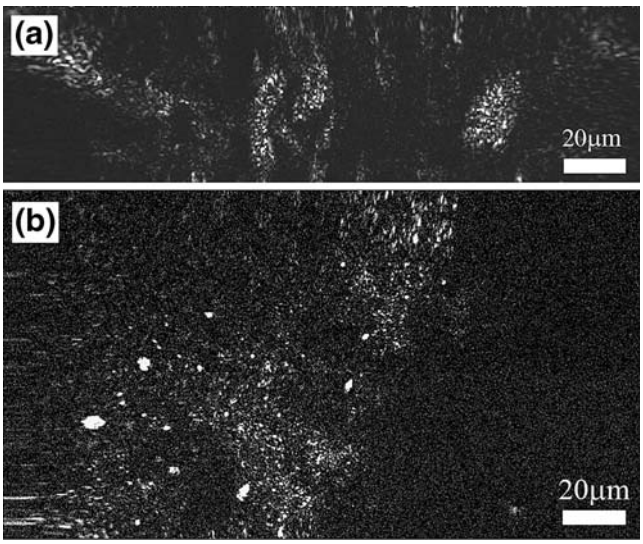

Fig. 7 MEMS Confocal images of biological samples. (**a**) *In vitro* oral porcine tissue treated with acetic acid, obtained using single-sided scan on the outer microscanner axis. Field of view is 200 μm×55 μm approximately; (**b**) *In vivo* human fingernail. Cell nuclei and cell borders are visible. Field of view is 200 μm×110 μm. Videos of samples were acquired at 3.5–5.0 frames per second

antibodies specific to cancerous lesions, to serve as imaging contrast agents (Bugaj et al. 2001; Hsu et al. 2004; Nida et al. 2005; Srinivas et al. 2001). Such fluorescence detection schemes can potentially exhibit dramatically higher detection sensitivity and specificity, if the associated drug delivery problems can be adequately addressed. With no changes to our handheld probe and only minor modifications to the proximal optical system, we can perform fluorescence confocal microscopy *in vivo* to leverage the advantages of such contrast agents.

5 Conclusions

High-reflectivity two-axis MEMS microscanners serve as an enabling technology to develop miniaturized, portable, battery-powered, single-fiber reflectance confocal microscopes for *in vivo* biopsy-free early precancer detection based on direct visualization of changes in sub-cellular morphology of diseased tissues. Our probe is demonstrated to acquire video of *in vivo* biological samples at 3.5–5.0 frames per second over a 200 μm×110 μm field-of-view with 0.80 μm, 9.55 μm lateral and axial resolution respectively. The 4.8 mm distal tip outer diameter forward-imaging probe configuration integrating miniature optical elements and flexible electrical routing allows maneuverability and unrestricted access for imaging in biological sites such as the oral cavity and cervix. Future optimizations of the device will include improving mirror diameter-scan angle product while further miniaturizing the system for Point-of-Care (POC) endoscopic diagnostics of internal human organs.

Acknowledgments Financial support for this research from the Wallace H. Coulter Foundation Early Career Award 2006–08 is gratefully acknowledged. The silicon microscanners were fabricated at Stanford Nanofabrication Facility (supported by National Science Foundation grant ECS 9731293) and Microelectronics Research Center at University of Texas at Austin (supported by National Science Foundation grant ECS 0335765), under the National Nanofabrication Infrastructure Network. The authors wish to thank Dr. H. J. Shin, Dr. M. C. Pierce, and Prof. R. Richards-Kortum with Department of Bioengineering, Rice University, for providing the miniature objective system and access to their confocal imaging setup.

References

American Cancer Society, Cancer Facts and Figures (2007)

Cancer Research UK, CancerStats Reports: Worldwide Cancer (2005)

J.E. Bugaj, S. Achilefu, R.B. Dorshow, R. Rajagopalan, Novel fluorescent contrast agents for optical imaging of *in vivo* tumors based on a receptor-targeted dye-peptide conjugate platform. J. Biomed. Opt. **6**, 122 (2001)

K.D. Carlson, Fiber Optic Confocal Microscope: *In Vivo* Precancer Detection, Ph.D. Dissertation, University of Texas at Austin (2006)

K.D. Carlson, M. Chidley, K.-B. Sung, M. Descour, A. Gillenwater, M. Follen, R. Richards-Kortum, *In vivo* fiber-optic confocal reflectance microscope with an injection-molded plastic miniature objective lens. Appl. Opt. **44**, 1792 (2005)

T. Collier, P. Shen, B.d. Pradier, K. Sung, R. Richards-Kortum, Near Real Time Confocal Microscopy of Amelanotic Tissue: Dynamics of Aceto-Whitening Enable Nuclear Segmentation. Opt. Express **6**, 40 (2000)

M.N. Cooke, J.P. Fisher, D. Dean, C. Rimnac, A.G. Mikos, Use of stereolithography to manufacture critical-sized 3D biodegradable scaffolds for bone ingrowth. J. Biomed. Materi. Res. **64B**, 65 (2002)

T. Dabbs, M. Glass, Fiber-optic confocal microscope: FOCON. Appl. Opt. **31**, 3030 (1992)

D.L. Dickensheets, G.S. Kino, Micromachined scanning confocal optical microscope. Opt. Lett. **21**, 764 (1996)

D.L. Dickensheets, G.S. Kino, Silicon-micromachined scanning confocal optical microscope. Journal of Microelectromechanical Systems **7**, 38 (1998)

R.A. Drezek, T. Collier, C.K. Brookner, A. Malpica, R. Lotan, R. Richards-Kortum, M. Follen, Laser scanning confocal microscopy of cervical tissue before and after application of acetic acid. Am. J. Obstet. Gynecol. **182**, 1135 (2000)

B.A. Flusberg, J.C. Jung, E.D. Cocker, E.P. Anderson, M.J. Schnitzer, *In vivo* brain imaging using a portable 3.9 gram twophoton fluorescence microendoscope. Opt. Lett. **30**, 2272 (2005)

L. Giniunas, R. Juskaitis, S.V. Shatalin, Scanning fiber-optic microscope. Electron. Lett. **27**, 724 (1991)

A.F. Gmitro, D. Aziz, Confocal microscopy through a fiber-optic imaging bundle. Opt. Lett. **18**, 565 (1993)

D. Hah, P.R. Patterson, H.D. Nguyen, H. Toshiyoshi, M.C. Wu, Theory and Experiments of Angular Vertical Comb-Drive Actuators for Scanning Micromirrors. IEEE J. Sel. Top. Quantum Electron. **10**, 505 (2004)

E.R. Hsu, E.V. Anslyn, S. Dharmawardhane, R. Alizadeh-Naderi, J.S. Aaron, K.V. Sokolov, A.K. El-naggar, A.M. Gillenwater, R. Richards-Kortum, A Far-red Fluorescent Contrast Agent to Image Epidermal Growth Factor Receptor Expression. Photochem. Photobiol. **79**, 272 (2004)

U. Krishnamoorthy, D. Lee, O. Solgaard, Self-aligned vertical electrostatic combdrives for micromirror actuation. Journal of Microelectromechanical Systems **12**, 458 (2003)

K. Kumar, K. Hoshino, H.-J. Shin, R. Richards-Kortum, X.J. Zhang, High-reflectivity two-axis vertical combdrive microscanners for sub-cellular scale confocal imaging applications. Proc. IEEE/LEOS International Conference on Optical MEMS and Their Applications 120 (2006)

S. Kwon, V. Milanovic, L.P. Lee, Vertical combdrive based 2-D gimbaled micromirrors with large static rotation by backside island isolation. IEEE J. Sel. Top. Quantum Electron. **10**, 498 (2004)

D. Lee, Design and fabrication of SOI-based micromirrors for optical applications, Ph. D. Dissertation, Stanford University (2007)

J.T.C. Liu, M.J. Mandella, H. Ra, L.K. Wong, O. Solgaard, G.S. Kino, W. Piyawattanametha, C.H. Contag, T.D. Wang, Miniature near-infrared dual-axes confocal microscope utilizing a two-dimensional microelectromechanical systems scanner. Opt. Lett. **32**, 256 (2007)

K.C. Maitland, H.-J. Shin, H. Ra, D. Lee, O. Solgaard, R. Richards-Kortum, Single fiber confocal microscope with a two-axis gimbaled MEMS scanner for cellular imaging. Opt. Express **14**, 8604 (2006)

R.G. McKinnell, R.E. Parchment, A.O. Perantoni, G.B. Pierce, The Biological Basis of Cancer, 2nd editionnd edn. (Cambridge University Press, New York, 2006), p. 14

D.L. Nida, M.S. Rahman, K.D. Carlson, R. Richards-Kortum, M. Follen, Fluorescent nanocrystals for use in early cervical cancer detection. Gynecol. Oncol. **99**, S89 (2005)

Y. Pan, H. Xie, G.K. Fedder, Endoscopic optical coherence tomography based on a microelectromechanical mirror. Opt. Lett. **26**, 1966 (2001)

W. Piyawattanametha, R.P.J. Barretto, T.H. Ko, B.A. Flusberg, E.D. Cocker, H. Ra, D. Lee, O. Solgaard, M.J. Schnitzer, Fast-scanning two-photon fluorescence imaging based on a microelectromechanical systems two-dimensional scanning mirror. Opt. Lett. **31**, 2018 (2006)

A.L. Polglase, W.J. McLaren, S.A. Skinner, R. Kiesslich, M.F. Neurath, P.M. Delaney, A fluorescence confocal endomicroscope for in vivo microscopy of the upper- and the lower-GI tract. Gastrointest. Endosc. **62**, 686 (2005)

H. Ra, W. Piyawattanametha, Y. Taguchi, D. Lee, M.J. Mandella, O. Solgaard, Two-Dimensional MEMS Scanner for Dual-Axes Confocal Microscopy. Journal of Microelectromechanical Systems **16**, 969 (2007)

M. Rajadhyaksha, R.R. Anderson, R.H. Webb, Video-rate confocal scanning laser microscope for imaging human tissues *in vivo*. Appl. Opt. **38**, 2105 (1999)

A.R. Rouse, A. Kano, J.A. Udovich, S.M. Kroto, A.F. Gmitro, Design and demonstration of a miniature catheter for a confocal microendoscope. Appl. Opt. **43**, 5763 (2004)

M.A.F. Scarparo, Q.J. Chen, A.S. Miller, J.H. Zhang, S.D. Allen, Mechanisms of carbon dioxide laser stereolithography in epoxy-based materials. J. Appl. Polym. Sci. **62**, 491 (1996)

H.-J. Shin, M.C. Pierce, D. Lee, H. Ra, O. Solgaard, R. Richards-Kortum, Fiber-optic confocal microscope using a MEMS scanner and miniature objective lens. Opt. Express **15**, 9113 (2007)

P.R. Srinivas, B.S. Kramer, S. Srivastava, Trends in biomarker research for cancer detection. The Lancet Oncol. **2**, 698 (2001)

R.H. Webb, Optics for laser rasters. Appl. Opt. **23**, 3680 (1984)

H. Xie, Y. Pan, G.K. Fedder, Endoscopic optical coherence tomographic imaging with a CMOS-MEMS micromirror. Sens. Actuators A Phys. **103**, 237 (2003)

L. Zhou, J.M. Kahn, K.S.J. Pister, Scanning micromirrors fabricated by an SOI/SOI waferbonding process. Journal of Microelectromechanical Systems **15**, 24 (2006)